Electric Power Systems Research 151 (2017) 115–124

Contents lists available at ScienceDirect

Electric Power Systems Research

journal homepage: www.elsevier.com/locate/epsr

On battery state estimation algorithms for electric ship applications

George S. Misyris[a,b], Antonios Marinopoulos[a,*,1], Dimitrios I. Doukas[b], Tomas Tengnér[a], Dimitris P. Labridis[b]

[a] ABB Corporate Research, 72178 Västerås, Sweden
[b] School of Electrical and Computer Engineering, Aristotle University of Thessaloniki, P.O. Box 486, 54124, Greece

ARTICLE INFO

Article history:
Received 22 November 2016
Received in revised form 17 March 2017
Accepted 8 May 2017

Keywords:
Batteries
Electric ships
Energy storage
Marine electrical equipment
State estimation algorithms

ABSTRACT

In the last decade increasing concerns about the environment, financial reasons based on fuel prices and application-specific operational challenges have been driving the development of electric propulsion and hybrid or full-electric ships. The use of battery energy storage systems (BESS), which are suitable for a broad range of ship applications with different requirements, can reduce the use of fossil fuels. In this paper the benefits of an onboard DC grid, as applied by ABB, are briefly presented. The integration of BESS and the challenges for ship applications are also discussed. The focus of this paper is on a parameter identification method for an electric model of a battery and the evaluation and validation of a battery state estimation method, in respect to the accuracy requirements for ship applications.

1. Introduction

Environmental, financial and operational reasons have been driving the development of electric propulsion and hybrid electric ships. Recently, the concept of all electric ships (AES) has been also introduced, due to many benefits, such as flexibility in space and weight allocation, more degrees of freedom in the power system layout, enhanced operating life, increased survivability and maintainability and overall efficiency, etc.[1]. Main drivers behind this are the naval applications [2], which involve special loads, e.g., the pulsed load of electromagnetic aircraft launchers, however other type of vessels also start to become interesting applications for electric ships with energy storage, like ferries [3,4].

The use of battery energy storage systems (BESS), which among others could be also charged by renewable energy sources mostly onshore, may reduce the use of fossil fuels for some ship applications. A broad range of specific applications, like peak shaving, capacity firming, spinning reserve, backup power and pure electric operation etc. are suitable for BESS, however they usually have quite different requirements. Vessel types specifically benefiting from such applications are offshore support vessels, drill rigs, ice breakers, tug boats and shuttle ferries.

For such hybrid or full electric ships, the optimization of the power system's operation relies heavily on the management of the energy storage. This has been already identified as a key issue for the control of the power system in AES [5], and it is for this reason that an accurate state estimation of the BESS is also so important. In specific, fast acting energy storage can compensate the lag of diesel generators and reduce their negative effects on power quality, while for longer time scales, an appropriate BESS could satisfy temporary increases in power demand, avoiding the need to start an additional generator, which would have to operate in partial load with low efficiency. The modular nature of BESS can also be seen as ideal for distributed energy storage, which can increase the reliability and flexibility of the complete power system, comparing to centralized storage, and is also easier to adjust to different types of load variation by reprogramming the inverters' control algorithms [5].

The technology of choice today is the Li-ion battery, which keeps improving continuously [6], while its cost is coming down quickly. The cost per kWh for electric vehicles (EV) batteries dropped by 35% during 2015 alone, according to Bloomberg New Energy Finance [7]. Much of this is driven by the economy of scale when battery manufacturers are ramping up production to meet increased demand from electric vehicles and stationary energy storage, but improvements in energy density is also an important factor. This increased interest in batteries for EVs in combination with environmental and energy issues is reflected to the recent work of a number of researchers [8–11].

* Corresponding author.
E-mail address: antonis.marinopoulos@ieee.org (A. Marinopoulos).
[1] A. Marinopoulos is now employed by the Joint Research Centre of the European Commission, Directorate C – Energy, Transport and Climate, Petten, The Netherlands.

http://dx.doi.org/10.1016/j.epsr.2017.05.009
0378-7796/

Depending on the system requirements for a BESS in a marine application stated by power profile, design lifetime, footprint and safety, etc., Li-ion batteries based on lithium nickel manganese cobalt oxide (NMC), lithium nickel cobalt aluminum oxide (NCA) or Li-phosphate (LFP) cathodes and carbon or Li-titanate (LTO) anodes may be chosen. Different battery systems have their respective strengths and weaknesses in terms of cost, charge and discharge rate capabilities, calendric and cyclic lifetimes and safety. That said, most BESS have to be designed with a sufficient initial over-sizing in order to cope with the fade in energy capacity and/or power capability over its lifetime. A marine BESS is typically comprised by one or more parallel strings with a nominal voltage in the range of 700 and 1000 V. Strings are paralleled to meet energy capacity and power capability requirements.

In this paper, an overview of an onboard DC system, as applied by ABB, is briefly presented and its benefits versus AC are shortly discussed. The integration of BESS along with some technical requirements and challenges for marine applications are also mentioned. The focus is on a parameter identification method for a typical battery model, and on a capacity and state-of-charge estimation using a combination of algorithms. The estimation method is validated with experimental results from lab measurements and shown to provide good accuracy. A discussion on the method's challenges to make it robust for demanding ship applications is also done.

2. BESS integration into an onboard DC system

There are many ways to integrate a BESS into the electric power system of a ship, in terms of circuit configuration, hardware interface and control. For example, even though the BESS is usually interfaced to the power distribution grid with its own power converter, it can also be connected directly to the DC-link of the electric propulsion system, eliminating the need for a DC/DC converter, but increasing the size of the frequency converter and the propulsion inverter that have to control the voltage of the DC-link to control the state-of-charge (SOC) of the BESS [12].

In the last years, the onboard DC grid is being adopted for various applications. For example, its advantages versus traditional AC systems regarding dynamic positioning operation of offshore support vessels (OSV) include improved efficiency, optimization of operation and fast ramping connected with the integration of energy storage [13]. In Fig. 1, an onboard DC distribution system including the BESS, as applied by ABB [14], can be seen in high-level detail. The main benefits from including a battery system are the reduction of fuel consumption and emissions, but also the improvement of the dynamic response of the system, compared to a diesel-electric generator, and the increased availability due to the instantaneous availability of energy back-up source.

The onboard DC grid in general provides a highly efficient power distribution system that allows a wide range of sea-faring vessels to cut their fuel consumption, as well as incorporate DC energy sources, such as solar PV panels and fuel cells, and of course BESS. Based on a recent analysis from ABB [14], the implementation of DC grid may reduce the electrical equipment footprint and weight of up to 30% and the fuel consumption and emissions by 20%. In fact, tests made in Dina Star, an offshore platform supply vessel outfitted with ABB's onboard DC grid, in 2014, identified a reduction of specific fuel oil consumption of up to 27% [15]. It has to be noted, that these improvements were the result of the onboard DC grid only, not taking into consideration any extra benefit from BESS integration.

BESS enabled vessels may be highly dependent on their energy storage systems to meet backup power requirements, dynamic performance and overall power system stability. Consequently, it is of key importance to ensure that the BESS at every moment have the capability to meet even the worst case scenarios. This is achieved by state estimation, i.e., SOC and state-of-health (SOH) estimation. Accurate battery state estimation is important since not only does it reflect the battery performance but it also enables appropriate, application-driven control actions. Moreover, information from the state estimation, both SOC and SOH, can be integrated into the onboard diagnostics and maintenance system of the ship. State estimation techniques can be broadly categorized in: direct measurement methods, book-keeping estimation, adaptive systems and hybrid methods.

3. Battery cell modeling

In this section, the battery cell modeling and the main phenomena that need to be taken into account for an accurate model, i.e., the relationship between the open circuit voltage (OCV) and the SOC, the hysteresis effect, the temperature and the charge/discharge current rate, and the capacity degradation, are described. In general and in its simplest form, a battery model can be expressed as a capacitor, whose capacity is equal to the real capacity of the battery. Considering the internal resistance of the battery, a resistor is added in series with the capacitor to simulate the instant drop of the battery voltage, after a current pulse. The capacitor and the resistance simulate the steady state of the battery. In order to describe the dynamic response of the battery (relaxation effect) after a current pulse, series connected RC branch(es) is/are used. A higher number of RC branches can give higher accuracy to the battery model, but also increases the complexity of the battery model. The efficient number of the RC branches, considering the complexity and the accuracy is regarded to be two [16], but in this work to make the model simpler only one RC branch, which gives also adequate results [17], is used. The choice of the number of RC branches is a trade-off between accuracy and complexity. Complexity refers to the computational effort that the algorithms add to the system operation, especially for an online application, which is also translated into increased computational burden as well as cost. Moreover, the proposed ECM is mostly dependent on the OCV–SOV curve and especially within the area of operation (0.1–0.9 SOC), a fact that makes it rather generic and universal and not only for Li-ion batteries. Consequently, considering the additional complexity, especially for online applications, to use a second (or more) RC branch for achieving a rather small accuracy improvement, the modeling with only 1 RC branch for this kind of batteries and applications is justified as more appropriate.

3.1. OCV–SOC relationship

The OCV has a non-linear relationship with the SOC and this non-linearity makes the battery parameter identification and the state of charge estimation rather challenging in terms of the stability and performance of the battery model. Therefore, although for modeling purposes the relationship between the OCV and the SOC could be considered as static, independent of the battery aging and the current rate, it can be shown that in reality it changes for different temperatures, especially below 0 °C. In order to deal with this non-linearity, the average OCV–SOC curve is divided into linear segments. In an approach similar to [18], to find the appropriate number of linear segments the first and second derivative of the OCV versus SOC have been used. The analysis resulted in 18 linear segments i.e., 10 linear segments from 0 to 0.2 of SOC and eight segments from 0.2 to 1.0 of SOC. This non-uniform distribution of linear segments across the OCV–SOC curve has been performed in order to deal with the high non-linearity of the OCV–SOC relationship observed for SOC levels below 0.2. Based on the fact that for normal C-rates the operation point moves "slowly" along the

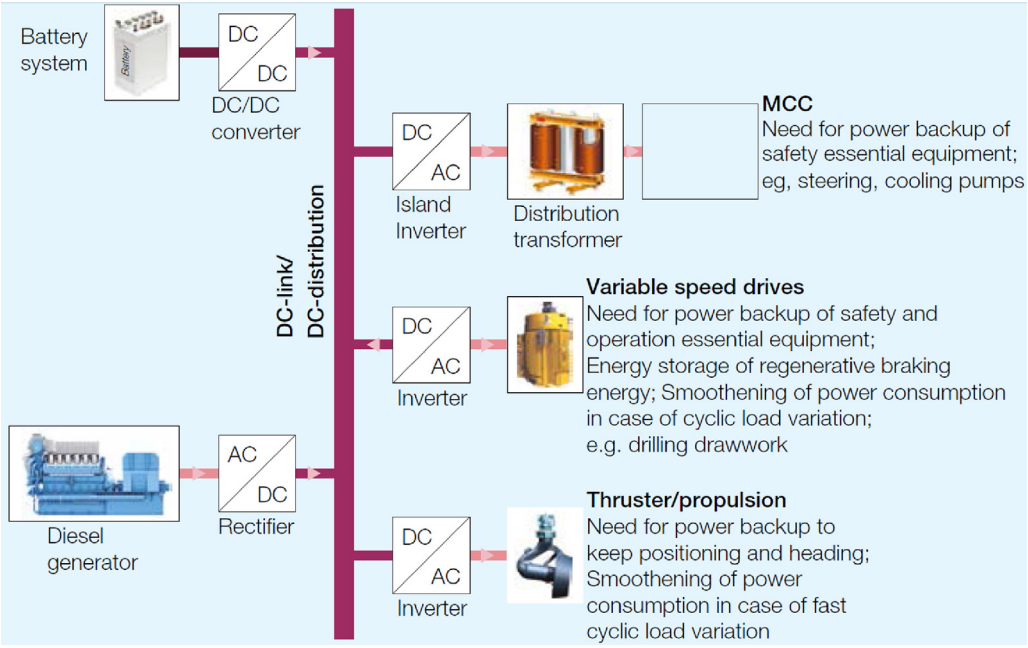

Fig. 1. Battery system connected through a DC/DC converter to a DC link in a hybrid power plant. (For interpretation of the references to color in this figure citation, the reader is referred to the web version of this article.)

OCV–SOC curve, a piece-wise linear relationship between OCV and SOC at each operation point of the battery can be considered. The equation which describes the OCV–SOC relationship for each of the linear segments [19] has the below generic form:

$$V_{OC} = b_0 + b_1 \cdot \mathrm{SOC} \tag{1}$$

where b_0 is the y-intercept and b_1 the slope of the linear equation.

3.2. Hysteresis effect

The equilibrium potential is higher at the charging process than that at the discharging process. Therefore we can infer that the equilibrium potential depends on the operation history of the battery during the charging and discharging process [20]. In this paper, the average of the equilibrium potentials of charging and discharging is considered to simplify the model.

3.3. Temperature effect and C-rate

Most of the researchers until now have been trying to estimate the parameters of the battery based on fixed conditions for temperature and current by identifying them offline. However, this puts a limitation using the model for real-time applications, where offline measurements are not available, but also for different kind of batteries, since each cell of a battery might present different characteristics, even if it is from the same manufacturer. As shown in [18], without change in temperature or current-rate the battery parameters can change as much as 800% and if we add on this the aging effect this difference can be even higher, so the estimation of SOC may be very inaccurate.

3.4. Capacity degradation

The maximum (nominal) capacity Q of a battery cell can be defined by the following equation:

$$\int_{t_1}^{t_1} \frac{\eta i(\tau)}{3600} d\tau = Q(\mathrm{SOC}(t_2) - \mathrm{SOC}(t_1)) \tag{2}$$

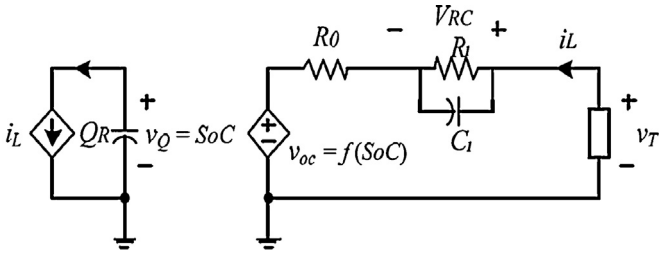

Fig. 2. Battery-equivalent circuit.

where η is the coulombic efficiency, $i(\tau)$ the current at time τ, Q the capacity, and $\mathrm{SOC}(t_1)$ the state of charge at t_1. It is obvious that Eq. (2) has a linear structure of $y = Qx$. An accurate estimation of the battery capacity is very important, in order to face the capacity fading as the battery ages. However, it is difficult to measure the battery capacity directly, thus some appropriate methods need to be applied in order to estimate it. As shown in [21] there are three kind of methods for capacity estimation: analytical, computational intelligence-based and model-based. In this paper, the model-based method, in which the SOC estimation and maximum capacity are based on battery models is used, and the total least squares (TLS) algorithm is implemented, to deal with the error being added to the system during the estimation processes.

3.5. Equivalent circuit model

In Fig. 2, the battery equivalent circuit model is presented. The RC branch simulates the relaxation effect of the battery, which represents the slow convergence of the battery voltage to its equilibrium after hours of relaxation following charging/discharging. The parameters of the RC branch, R_1 and C_1, respectively, change with SOC, temperature and aging. In order to bridge SOC to the OCV voltage, a voltage-controlled source is used. This source describes the nonlinear relationship between OCV and SOC, which is static. When the battery is being charged or discharged, current-controlled source I_L is used so that the SOC of the battery changes dynamically. The series resistance R_0 simulates the instant voltage

after charge/discharge of the battery. It represents the electrochemical process of the battery due to the electrolyte and the inter-phase resistance. R_0 also changes with SOC, temperature and the aging effect of the battery and is a great indication of battery SOH.

As pre-mentioned, one RC branch in the equivalent circuit is used, so the state-space equations, which describe the battery operation are:

$$\begin{cases} \begin{bmatrix} \dot{SOC} \\ \dot{V_{RC}} \end{bmatrix} = \begin{bmatrix} 0 & 0 \\ 0 & \frac{-1}{R_1 C_1} \end{bmatrix} \begin{bmatrix} SOC \\ V_{RC} \end{bmatrix} + \begin{bmatrix} \frac{1}{Q_R} \\ \frac{1}{C_1} \end{bmatrix} i_L \\ V_T = \begin{bmatrix} b_1 & 1 \end{bmatrix} \begin{bmatrix} SOC \\ V_{RC} \end{bmatrix} + R_0 i_L + b_0 \end{cases} \tag{3}$$

where the state variables of the system are the SOC and the voltage drop on the RC branch. The only known variables from this state-space system are the current and the output voltage. In order to estimate the SOC and V_{RC} we need first to identify the unknown battery parameters. Since we can extract b_1 and b_0 from the OCV–SOC curve and QR does not affect the other parameters [22], apart from b_1 that is anyway known, the only unknown parameters are R_1, C_1 and R_0.

4. Parameter identification and SOC/capacity estimation

This section has three parts: in the first part the parameter identification method for the above mentioned battery model is described, in the second part the SOC estimation is presented and in the third part the capacity estimation algorithms are given. Based on the model shown in Fig. 2, the transfer function of the system, from which the parameters of the equivalent circuit are extracted is:

$$\frac{\mathbf{Y}(s) - b_0}{\mathbf{U}(s)} = \frac{R_0 s^2 + ((b_1/Q_R) + (1/C_1) + (R_0/R_1 C_1 Q_R))s + (b_1/R_1 C_1 Q_R)}{s(s + (1/RC))} \tag{4}$$

Then, using bi-linear transformation($s \rightarrow \frac{2}{T}\frac{z-1}{z+1}$), we get the discrete transfer function (5) with sample time T. By implementing a recursive least squares (RLS) filter with forgetting factor we can estimate the coefficients of the discrete transfer function and then identify the parameters of the battery. The forgetting factor λ is a parameter used in the RLS filter, which takes values between 0 and 1, giving exponentially less weight to older error samples. The smaller the λ is, the smaller is the contribution of previous samples to the co-variance matrix, making the filter more sensitive to recent samples. It is also worth mentioning that the sample time is very important for the parameter identification. As shown in [23], the sample time of the data (input/output) affects the parameter identification, so we choose a sample time to be greater than 0.5 s to maintain a good performance for the parameter identification.

$$\frac{\mathbf{Y}(z^{-1}) - b_0}{\mathbf{U}(z^{-1})} = \frac{c_0 + c_1 z^{-1} + c_2 z^{-2}}{1 + a_1 z^{-1} + a_2 z^{-2}} \tag{5}$$

4.1. Parameter identification

In order to identify the battery parameters we use the RLS filter, with its limitation that poor excitation of the system can lead to the co-variance "wind-up problem" [24] and the different battery dynamics [25]. In terms of this problem, we propose changing the value of the forgetting factor based on the excitation of the system and implementing RLS with different forgetting factor for the parameters according to the system dynamics, so that we estimate the battery parameters. Specifically, when the excitation of the battery reduces, the forgetting factor increases and tends to unity to enhance the performance of the estimator. On the other hand, when the excitation of the battery is high, we want the old information continuously to be forgotten, due to the new dynamic information that keeps coming in, so the forgetting factor reduces and tends to a lower value. Therefore, the forgetting factor depends on the level of excitation of the system and ranges between 0.96 and 1.00.

On the battery equivalent circuit the series resistor and the parameters of the RC branch vary with different rate, so in order to estimate them accurately we use two different values for the forgetting factor: one higher value, when we estimate the series resistor on the battery-equivalent circuit, and one lower value when we estimate the parameters on the RC branch. Both of these values for the forgetting factor are between 0.96 and 1.00 and change, as described above, based on the battery excitation. For the sake of briefness, the RLS algorithm is not presented, since it is available and is described extensively in [24].

Afterwards, we estimate the discrete transfer function coefficients, using the equations found in [22]. In order to deal with some overshoot or undershoot that may occur, when we use the RLS with forgetting factor, we put limits to the parameters of the equivalent circuit. We only put limit 0 to 1 Ω to the series resistance, because it changes with a very high rate, and that causes some overshoots and undershoots, which affect the SOC estimation and thus the capacity estimation, as well. So we can see that by using the voltage output and the current we can identify the battery parameters and how they vary with the aging and the temperature, since the voltage output and the current carries the information for the battery.

4.2. SOC estimation

Having identified the battery parameters, we then proceed to the SOC estimation. Since we linearize our battery system at every time step, we can use the linear Kalman Filter algorithm, which is described analytically in [26]. The state equations of the battery are:

$$\begin{cases} \dot{x} = Ax + Bu \\ y = Cx + Du + b_0 \end{cases} \tag{6}$$

where $x_1 = SOC$, $x_2 = V_{RC}$, $A = \begin{bmatrix} 0 & 0 \\ 0 & \frac{-1}{R_1 C_1} \end{bmatrix}$, $B = \begin{bmatrix} \frac{1}{Q_R} \\ \frac{1}{C_1} \end{bmatrix}$, $C = \begin{bmatrix} 1 & 0 \\ 0 & b_1 \end{bmatrix}$, $D = R_0$, $u = I_L$, $y = V_T$ and $x = \begin{bmatrix} x_1 \\ x_2 \end{bmatrix}$.

Based on the theory of linear Kalman filters, the co-variance calculation is independent of the state, so we can infer that the capacity degradation does not affect the SOC estimation when using the linear Kalman Filter. The solution of the Riccati equation in a time invariant system converges to steady state co-variance if the matrices A, C are observable, which in our case depends on b_1, R_1 and C_1. Therefore, we conclude that an accurate parameter identification, i.e., R_1 and C_1 values, is crucial for the SOC estimation.

The equations for the implementation of the algorithm for the SOC estimation can be divided into 5 steps, which are repeated at each time update, after the initialization of the state matrix, the co-variance and the process and measurement noise:

1. State estimate time update:

$$\hat{x_k^-} = A_{k-1}\hat{x_{k-1}^+} + B_{k-1}u_{k-1} \tag{7}$$

2. Error co-variance time update:

$$\sum \hat{x_k^-} = A_{k-1} \sum \hat{x_{k-1}^+} A_{k-1}^T + \sum w \tag{8}$$

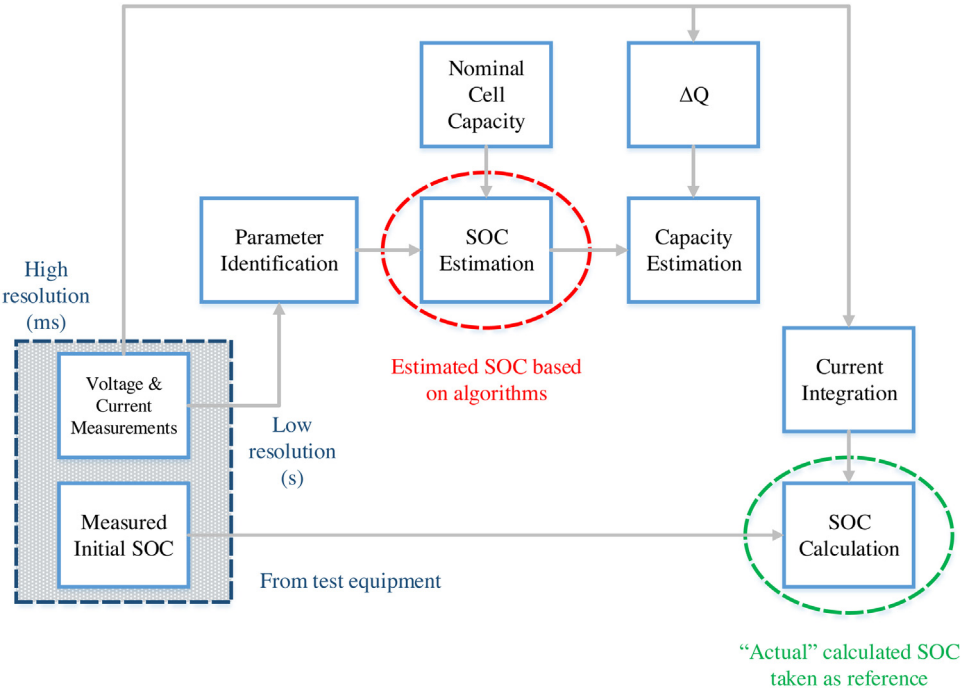

Fig. 3. Overview of the proposed model. (For interpretation of the references to color in this figure citation, the reader is referred to the web version of this article.)

3. Kalman gain matrix:

$$L_k = \sum \hat{x_k^-} C_k^T [c_k \sum \hat{x_k^-} C_k^T + \sum u]^{-1} \quad (9)$$

4. State estimate measurement update:

$$\hat{x_k^+} = \hat{x_k^-} + L_k[y_k - C_k \hat{x_k^-} - D_k u_k] \quad (10)$$

5. Error co-variance measurement update:

$$\sum \hat{x_k^+} = (I - L_k C_k)\hat{x_k^-} \quad (11)$$

4.3. Capacity estimation

Capacity update is crucial when we want to model the operation of the battery as it ages, because knowing the capacity (together with the increase of the internal resistance) will provide information about the SOH of the battery. In order to estimate the capacity degradation, we use total least squares (TLS) algorithm that, as applied for the estimation of the battery capacity, tries to find the slope of the equation $y = Q\hat{x}$ where $x = \mathrm{SOC}(t_2) - \mathrm{SOC}(t_1)$ and $y = \int_{t_1}^{t_1} \frac{\eta i(\tau)}{3600} d\tau$. We will assume $\eta = 1$ at all values of current and temperature which is inside the normal operation according to the manufacturer. For operations outside of the normal of this range, like low temperature and high C-rate, η must be specifically adjusted according to the analysis presented in [27]. The algorithm we use for the capacity estimation is an extension of the TLS algorithm and has been proposed in [28]. Due to its simplicity, no need to store any value, it can be very easily computed in a recursive manner, which makes it suitable for the MATLAB/Simulink® environment. The steps of the algorithm are extensively described in [28].

4.4. Discussion

The main novelty in the proposed model is the introduction of different forgetting factors, which has not been presented in literature yet. The use of different forgetting factors enables more accurate SOC and capacity estimation results, since the parameter identification process, which is of key importance considering the battery states estimation becomes more accurate. Moreover, a fully detailed model regarding the necessary to estimate parameters during the whole lifetime of the battery is presented.

In case of ships, several BESSs are connected in series or in parallel as a battery set a fact that makes important that the proposed model simulates the battery and the battery-cell as black boxes. The measured voltage and current of the battery are used from the algorithms as inputs to estimate the states and identify the parameters. The measured voltage of either a battery pack or a battery cell is being simulated and processed in the same way from the algorithms in case the battery cells are in series. Same goes for the current in case the battery cells are in parallel. The main factor that affects the states estimation is the OCV–SOC curve considering the voltage level. OCV–SOC curve can be extracted for a battery pack accurately in the same way that is described for a battery cell. Consequently, the proposed model is generic and could be applied in case of both battery packs and/or battery cells, as long as an accurate OCV–SOC curve can be extracted.

5. Evaluation and experimental validation

In order to verify the accuracy of the proposed model we have setup two simulation tests, testing its efficiency on two different types of Li-ion batteries at different excitation levels of the battery. Firstly, based on the analysis presented in Sections 3 and 4, an overview of the proposed model is illustrated in Fig. 3. Fig. 3 corresponds to a block diagram showing two parallel paths: one for simulation with algorithms and one for test results. They both start with test measurements for V and I and then the algorithms, considering these, estimate the states, while for the experimental results the SOC for example comes from the current integration, due to high resolution and accuracy. In principle the SOC and capacity estimation are sent to the DC grid controller. The two tests have been performed at varying temperatures and different current rates. Table 1 shows the nominal characteristics of the two tested batteries. For the tests we used the LifeTest SBT0550 battery cell

Table 1
Batteries nominal characteristics.

	Battery 1	Battery 2
Maximum capacity (Ah)	25.90	20.00
Nominal voltage (V)	4.2	2.7
Chemistry	Li-ion NMC-LMO/graphite	Li-ion LTO/mixed oxide

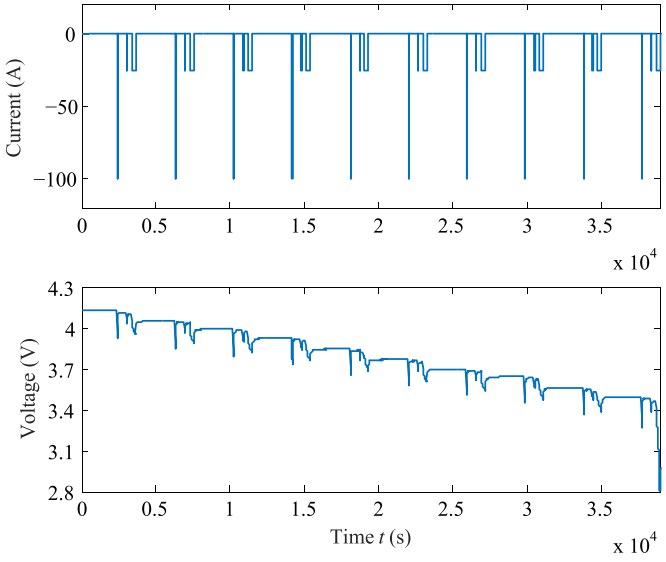

Fig. 4. Current and voltage profile for the first experiment. (For interpretation of the references to color in this figure citation, the reader is referred to the web version of this article.)

tester from PEC Corporation, which offers a very accurate current measurement at a rate of 1 ms. This current measurement is used to integrate current for Coulomb counting (CC) SOC estimation and to compare to the proposed state estimation method.

In case of online applications, load profiles can be separated into two major categories, i.e., either with high or with poor excitation [24]. The following experiments have been chosen, in order to investigate the accuracy and the efficiency of the proposed model under such varying loading conditions. Note that the dynamic loads are not necessarily divided based on the application but based on the input dynamic change. Consequently, considering load-profiles with such different characteristics as the ones presented in Figs. 4 and 5 , could be easily translated into an assessment of two different ship loads as the ones described in Section 1. Voltage and current for both examined cases have been captured during lab measurements. Furthermore, the reference SOC that is to be used as a benchmark in order the SOC estimation results to be compared with, has been also derived from experimental results.

The first experiment that we set up for Battery 1 is a full discharge of the battery. The specific load profile is given in Fig. 4, which illustrates a pulse test from 1 to 0 SOC, with 10 s and 40 s pulses made at 10% SOC increments to capture the dynamic response of the battery at each SOC increment. In the upper plot of Fig. 4 the imposed discharge current pulses are presented, while in the bottom the voltage response of the battery cell is illustrated. According to the manufacturer, the battery cell can have a maximum current-rate of 5 C and given that in this case 1 C equals 25.9 A (nominal cell capacity 25.9 Ah), 5 C leads to a current of almost 125 A. In case of the experiment presented in Fig. 4, a maximum current rate of 4 C is measured, therefore 100 A. We can think of this experiment as a low excitation input in order to see how the RLS with variable forgetting factor can adjust the "wind-up" of the co-variance matrix.

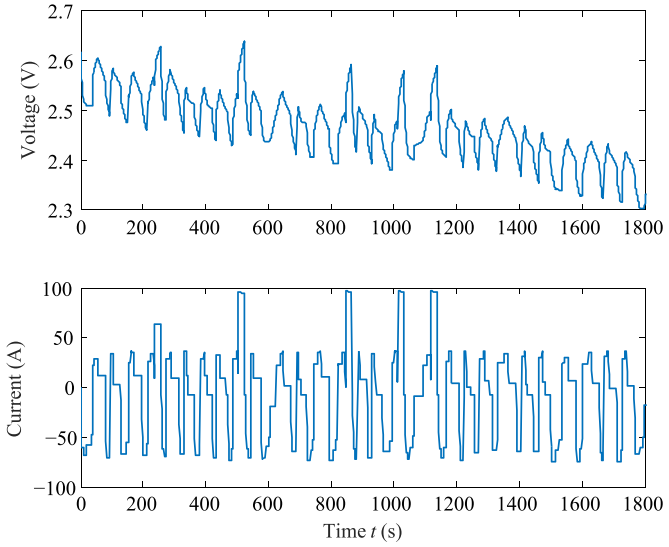

Fig. 5. Current and voltage profile for the second experiment. (For interpretation of the references to color in this figure citation, the reader is referred to the web version of this article.)

Table 2
Forgetting factor range.

	R_0	R_1,C_1
λ_{exp1}	[0.995 0.99986]	[0.98 0.99986]
λ_{exp2}	[0.992 0.99996]	[0.96 0.99996]

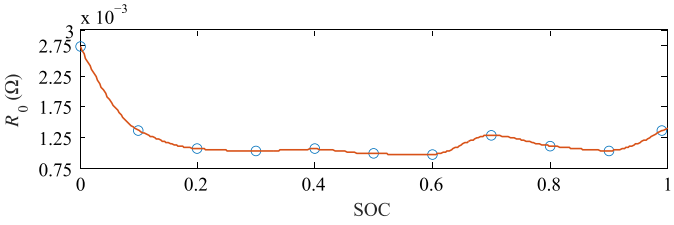

Fig. 6. R_0–SOC relationship on the first experiment. (For interpretation of the references to color in this figure citation, the reader is referred to the web version of this article.)

The second experiment is a dynamic load with high excitation and different current rates, which is implemented to Battery 2. Current and voltage profile for the second experiment are given in Fig. 5. In the upper and bottom plots of Fig. 5 the imposed discharge current pulses and the voltage response of the battery cell are depicted, respectively. For this experiment, the maximum current rate equals again 5 C, however for this case 1 C equals 20 A (nominal cell capacity 20 Ah). In order to validate the algorithm for the capacity estimation we applied the same load to Battery 2 for a long period of time. Also we should mention that on this experiment the temperature varies between 20° and 30° so we can estimate our system's dependency on temperature. A voltage drop within one second is considered instantaneous, therefore this as the sample time in our model [29].

Specifically, on the first experiment there is a slow changing current profile, with currents equal to 25.9 A and 100 A. The temperature on this experiment slowly changes and the discharging process lasts 39,842 s. In the following figures we present the parameter identification and the SOC estimation. Since we only discharge the battery once we do not present any capacity estimation. The forgetting factor variance is presented in Table 2. In Figs. 6–8 we present the curves of the battery parameters versus SOC, which have been identified using RLS with multiple forgetting factor.

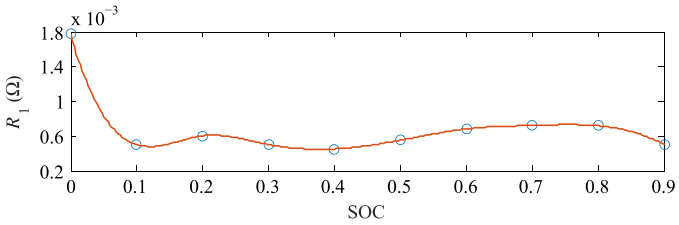

Fig. 7. R_1–SOC relationship on the first experiment. (For interpretation of the references to color in this figure citation, the reader is referred to the web version of this article.)

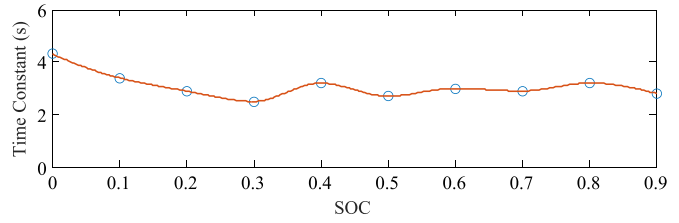

Fig. 8. Time constant–SOC relationship on the first experiment. (For interpretation of the references to color in this figure citation, the reader is referred to the web version of this article.)

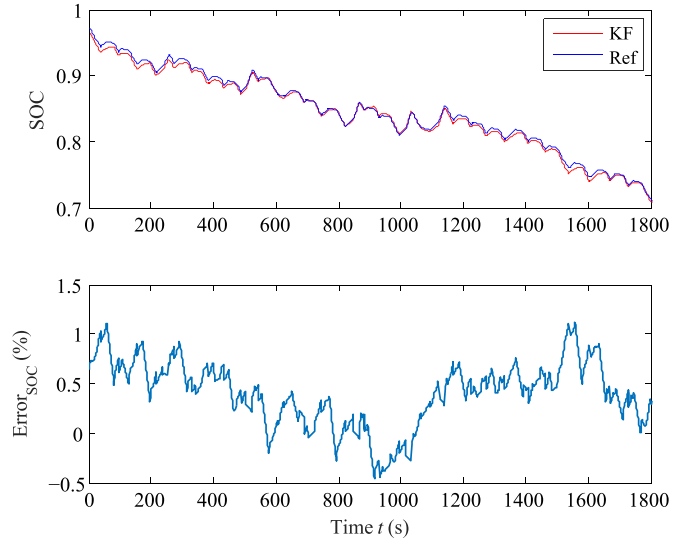

Fig. 9. SOC estimation and SOC error for the first experiment. (For interpretation of the references to color in this figure citation, the reader is referred to the web version of this article.)

As for the SOC estimation, the results show that it is very accurate at the higher level of SOC, but as the depth of discharge increases, the non-linearity increases, as well. Thus, the error in SOC increases since the equivalent circuit model cannot simulate very accurately the dynamic response of the battery and furthermore an error is being added to the estimation because the linear Kalman Filter is not able to do the estimations of states when there is high non-linearity, as shown in Fig. 9. Therefore, since the linear Kalman Filter is not efficient under 20% (as we will also see in the validation part), using simple CC method for the range 0–20% might actually give better results for the SOC estimation. This idea of using two different SOC estimation methods for different ranges of SOC, is under investigation for future work.

On the second experiment, as seen in Fig. 5, there is a much faster changing current profile, with currents varying from 0 to 5 C.

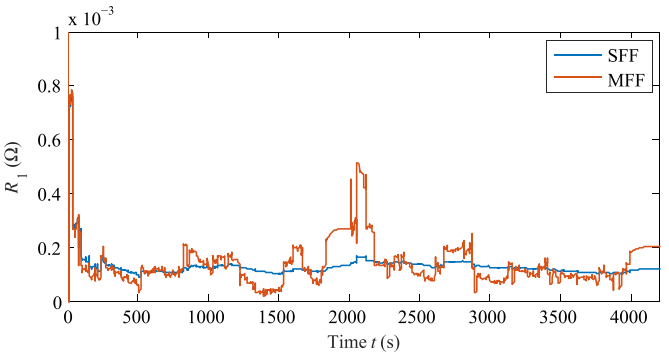

Fig. 10. Difference between R_1 identification using SFF and MFF. (For interpretation of the references to color in this figure citation, the reader is referred to the web version of this article.)

On this experiment the temperature changes very little, since the cell under test was inside a climate chamber. The charging and discharging lasted almost one week (for the capacity estimation), but for the sake of briefness, we will present only the first 1800 s of the experiment.

The fast changing currents on this experiment allow for checking the importance of using multiple values for the forgetting factor. As mentioned above, the forgetting factor (λ) gives the contribution of previous samples to the co-variance matrix. The smaller it is, the more sensitive it becomes to recent samples. For the proposed model, we want the series resistance to change much slower than the parameters of the RC branch at every new data that arrives as an input to our model, thus a higher value for the forgetting factor than the one that we set for the R_1 and C_1. This is because the RC branch simulates the relaxation effect, which means that they vary more than the series resistance with a much longer time constant. So with a lower value for the forgetting factor R_1 and C_1 change at every input, in order to capture the transient response of the battery. When the excitation of the system is slow we set a value very close to 1, since we do not expect our system states to change much. On Table 2 we can see the range of the forgetting factor values for this experiment, as well.

To illustrate the importance of using different values for the λ for estimating the different parameters, we conduct a comparison between single (SFF) and multiple forgetting factor (MFF). The reasons to apply MFF have been mentioned above, while applying SFF means that the value of λ still changes for different excitation, but is the same for estimating R_0, R_1 and C_1. For the MFF we apply the λ as mentioned in the previous paragraph, whereas for the RLS with SFF we chose to simulate the worst case, i.e., low λ for the R_0 estimation, which will give an accurate estimation for R_1 and C_1, but poor for the R_0, and high λ for the R_1 and C_1 estimation, which will give accurate estimation for the R_0 but poor for R_1 and C_1. In Figs. 10 and 11 we can see the difference of using SFF and MFF. If we choose SFF, we might end up to lose information of the variance of the parameters or even worse have great overshoots/undershoots of the parameters values, which may lead to greater error on the SOC estimation. The benefit of MFF is that the series resistance R_0 changes much slower than the parameters, R_1 and C_1, of the RC branch for every new data that arrives as an input to the model, thus a higher value for the forgetting factor λ than the one that is set for the R_1 and R_1, as indicated in Table 2 also. The algorithm that used to implement MFF is based on the work of [24]. Moreover, we present how the series resistance respond to the variances of the temperature.

As shown in Fig. 12, when the temperature is high the resistance decreases and when the temperature drops the resistance increases. As it is shown from the SOC estimation figures, our model

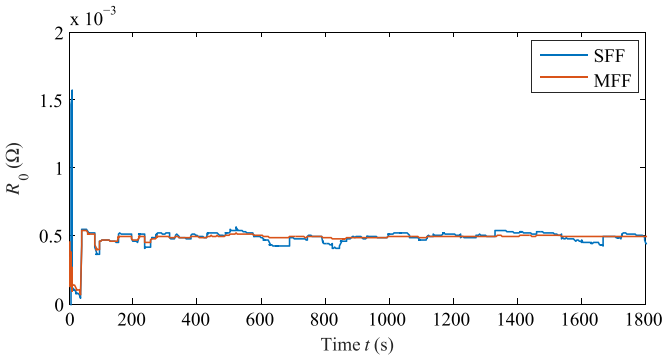

Fig. 11. Difference between R_0 identification using SFF and MFF. (For interpretation of the references to color in this figure citation, the reader is referred to the web version of this article.)

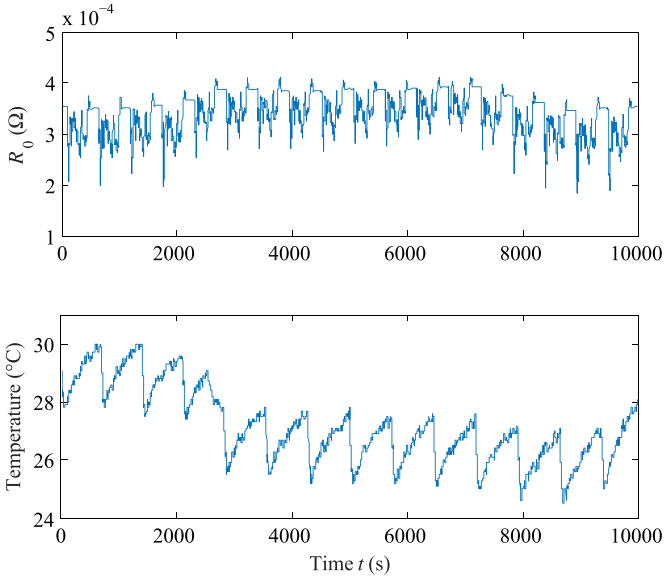

Fig. 12. R_0 identification considering the variance of temperature. (For interpretation of the references to color in this figure citation, the reader is referred to the web version of this article.)

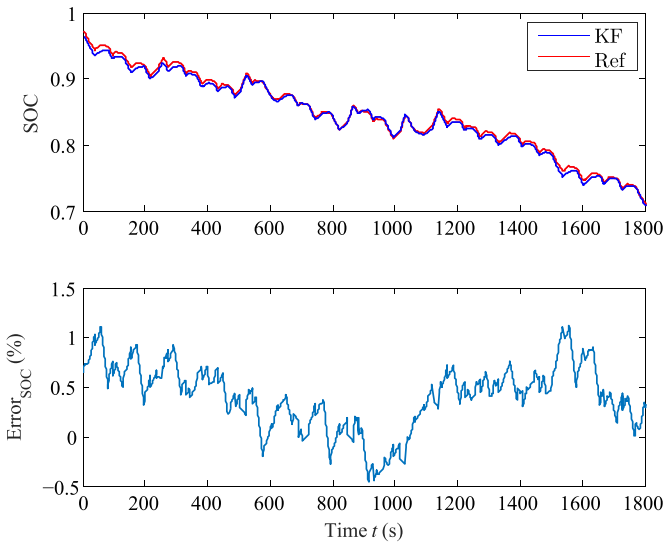

Fig. 13. SOC estimation without noise to the current. (For interpretation of the references to color in this figure citation, the reader is referred to the web version of this article.)

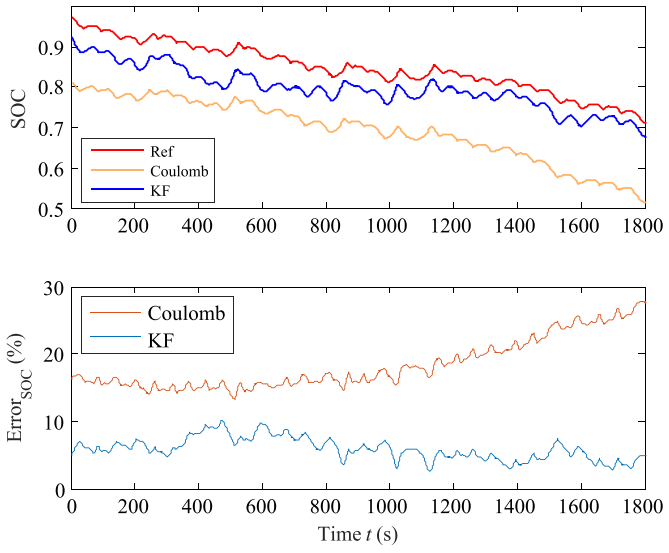

Fig. 14. SOC estimation with −10 A average noise to the current. (For interpretation of the references to color in this figure citation, the reader is referred to the web version of this article.)

gives very accurate results, with an error less than 2%, when we do not have current noise and less than 6% average when we have noise.

In Figs. 13–15 we can see three different simulations that we have set up for the SOC estimation. One is for the SOC estimation without any noise and the other two are for an average noise ±10 A to the current, a really extreme measurement error considered on purpose to validate the convergence of our algorithm to the true SOC. In the same Figures, and for the same noise in current measurement, the error (over 15%) for the simple CC method for SOC estimation is shown.

CC has been used as a reference, since it is a conventional method to estimate SOC and gives very accurate results in short term, right because PEC test equipment provides a very accurate current measurement and an internal current integration. Its main drawback is that in long term, due to SOC-drifting, SOC estimation may give bad results. Therefore it is essential the model to be able at any point of battery life to converge to the actual value of SOC considering also the battery capacity fading. That is why an initial noise in the initial SOC has been added, so that the main advantage of the proposed method to be pointed out, i.e., that the SOC estimation converges back to the reference value even when the algorithm is fed on purpose with an offset current. Note that in Figs. 14 and 15, the red curve (Ref) comes from the accurate internal CC method from the tester, but the yellow curve (Coulomb) refers to what the SOC estimation would have been if the CC method would have been used but with low resolution current input, i.e., the same that is used as an input to the algorithms.

Regarding the capacity estimation, as we can see from Fig. 16 the capacity has not dropped at all. This is due to the battery's chemistry, which presents a very long life cycle (in the range of 10,000 cycles). The capacity drop is 0.03% and we see the accuracy of the TLS algorithm.

6. Conclusions

In this paper we began with a short discussion about the benefits of including energy storage, in specific BESS, into the electrical network of hybrid and full-electric ships. A brief overview of an

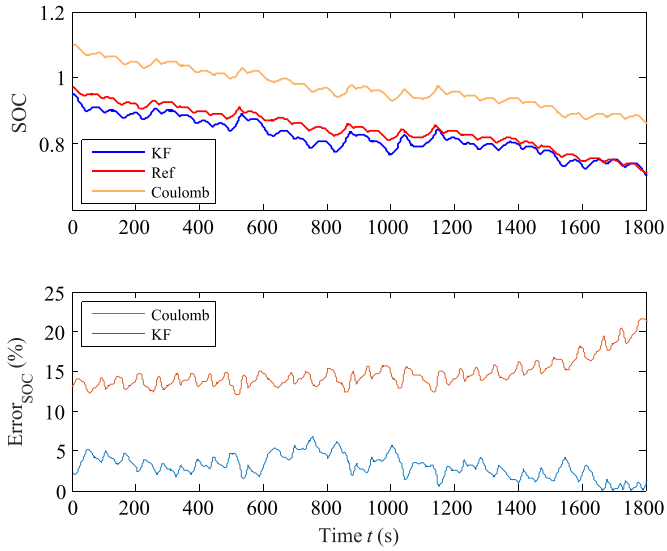

Fig. 15. SOC estimation with +10 A average noise to the current. (For interpretation of the references to color in this figure citation, the reader is referred to the web version of this article.)

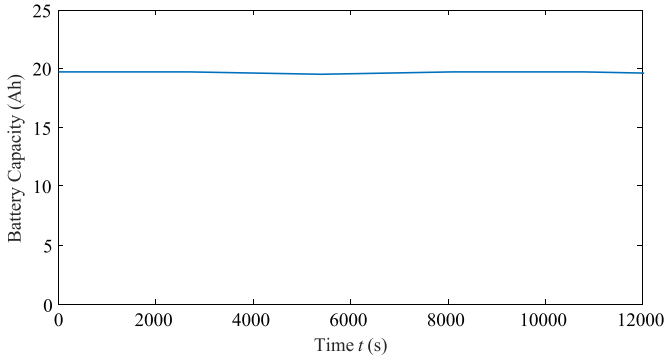

Fig. 16. Battery capacity estimation. (For interpretation of the references to color in this figure citation, the reader is referred to the web version of this article.)

onboard DC grid has been also presented, showing the improvements that it can bring in total system efficiency and the easier integration of BESS. The differences between onshore grid applications and onboard ship applications regarding safety and operation create a more challenging environment for the BESS. Thus, in order to exploit an integrated BESS for an optimized ship power system operation an accurate SOC estimation is crucial from technical, economic and safety point of view. We proposed a parameter identification method that uses RLS filter with multiple and variable forgetting factors for different parameters and a SOC and Capacity estimation based on Kalman filter and TLS algorithm, respectively. These were validated with test measurements in two different battery cells and the results showed a good fit, especially regarding the SOC and the capacity. Future work includes improvements of the parameter identification method, as well as the idea of using different SOC estimation for different SOC ranges to tackle the nonlinearity in lower SOC levels.

Acknowledgements

The authors would like to thank Stig Leira and John O. Lindtjørn from ABB Process Automation, Marine Applications Unit in Norway for their support.

References

[1] A. Vicenzutti, D. Bosich, G. Giadrossi, G. Sulligoi, The role of voltage controls in modern all-electric ships: toward the all electric ship, IEEE Electrific. Mag. 3 (2) (2015) 49–65, http://dx.doi.org/10.1109/MELE.2015.2413437.
[2] J.S. Thongam, M. Tarbouchi, A.F. Okou, D. Bouchard, R. Beguenane, All-electric ships – a review of the present state of the art, 2013 8th International Conference and Exhibition on Ecological Vehicles and Renewable Energies (EVER) (2013) 1–8, http://dx.doi.org/10.1109/EVER.2013.6521626.
[3] M. Bianucci, S. Merlino, M. Ferrando, L. Baruzzo, The optimal hybrid/electric ferry for the Liguria natural parks, OCEANS 2015 – Genova (2015) 1–10, http://dx.doi.org/10.1109/OCEANS-Genova.2015.7271474.
[4] Fuel-Efficient Fast Ferries in Carbon Fibre. http://www.braa.no/seasight (accessed 21.11.16).
[5] A. Monti, S. D'Arco, L. Gao, R.A. Dougal, Energy storage management as key issue in control of power systems in future all electric ships, International Symposium on Power Electronics, Electrical Drives, Automation and Motion, 2008, SPEEDAM 2008 (2008) 580–585, http://dx.doi.org/10.1109/SPEEDHAM.2008.4581218.
[6] K. Divya, J. Østergaard, Battery energy storage technology for power systems – an overview, Electr. Power Syst. Res. 79 (4) (2009) 511–520, http://dx.doi.org/10.1016/j.epsr.2008.09.017.
[7] Bloomberg New Energy Finance Summit. http://goo.gl/6KhSai (accessed 21.11.16).
[8] M. Ibrahim, S. Jemei, G. Wimmer, D. Hissel, Nonlinear autoregressive neural network in an energy management strategy for battery/ultra-capacitor hybrid electrical vehicles, Electr. Power Syst. Res. 136 (2016) 262–269, http://dx.doi.org/10.1016/j.epsr.2016.03.005.
[9] S. Hajforoosh, M.A. Masoum, S.M. Islam, Real-time charging coordination of plug-in electric vehicles based on hybrid fuzzy discrete particle swarm optimization, Electr. Power Syst. Res. 128 (2015) 19–29, http://dx.doi.org/10.1016/j.epsr.2015.06.019.
[10] M. ElNozahy, M. Salama, Studying the feasibility of charging plug-in hybrid electric vehicles using photovoltaic electricity in residential distribution systems, Electr. Power Syst. Res. 110 (2014) 133–143, http://dx.doi.org/10.1016/j.epsr.2014.01.012.
[11] A. Neffati, M. Guemri, S. Caux, M. Fadel, Energy management strategies for multi source systems, Electr. Power Syst. Res. 102 (2013) 42–49, http://dx.doi.org/10.1016/j.epsr.2013.03.008.
[12] S.Y. Kim, S. Choe, S. Ko, S.K. Sul, A naval integrated power system with a battery energy storage system: fuel efficiency, reliability, and quality of power, IEEE Electrific. Mag. 3 (2) (2015) 22–33, http://dx.doi.org/10.1109/MELE.2015.2413435.
[13] J.F. Hansen, J.O. Lindtjørn, K. Vanska, Onboard DC grid for enhanced DP operation in ships, in: Dynamic Positioning Conference, Marine Technology Society, 2011.
[14] ABB, BU Marine and Cranes: Energy Efficiency Guide, Tech. Rep., 2013.
[15] ABB: Tests Confirm Up To 27% Fuel Savings on Ships from Onboard DC Grid. http://goo.gl/xpYGDm (accessed 21.11.16).
[16] M. Chen, G.A. Rincon-Mora, Accurate electrical battery model capable of predicting runtime and I-V performance, IEEE Trans. Energy Convers. 21 (2) (2006) 504–511, http://dx.doi.org/10.1109/TEC.2006.874229.
[17] X. Hu, S. Li, H. Peng, A comparative study of equivalent circuit models for Li-ion batteries, J. Power Sources 198 (2012) 359–367, http://dx.doi.org/10.1016/j.jpowsour.2011.10.013.
[18] H. Rahimi-Eichi, F. Baronti, M.Y. Chow, Modeling and online parameter identification of Li-polymer battery cells for SOC estimation, 2012 IEEE International Symposium on Industrial Electronics (ISIE) (2012) 1336–1341, http://dx.doi.org/10.1109/ISIE.2012.6237284.
[19] H. Rahimi-Eichi, F. Baronti, M.Y. Chow, Online adaptive parameter identification and state-of-charge coestimation for Lithium-polymer battery cells, IEEE Trans. Ind. Electron. 61 (4) (2014) 2053–2061, http://dx.doi.org/10.1109/TIE.2013.2263774.
[20] H. He, R. Xiong, X. Zhang, F. Sun, J. Fan, State-of-Charge estimation of the Lithium-ion battery using an adaptive extended Kalman filter based on an improved Thevenin model, IEEE Trans. Veh. Technol. 60 (4) (2011) 1461–1469, http://dx.doi.org/10.1109/TVT.2011.2132812.
[21] T. Kim, Y. Wang, Z. Sahinoglu, T. Wada, S. Hara, W. Qiao, A Rayleigh quotient-based recursive total-least-squares online maximum capacity estimation for Lithium-ion batteries, IEEE Trans. Energy Convers. 30 (3) (2015) 842–851, http://dx.doi.org/10.1109/TEC.2015.2424673.
[22] H. Rahimi-Eichi, M.Y. Chow, Adaptive online battery parameters/SOC/capacity co-estimation, 2013 IEEE Transportation Electrification Conference and Expo (ITEC) (2013) 1–6, http://dx.doi.org/10.1109/ITEC.2013.6574502.
[23] S. Yuan, H. Wu, X. Ma, C. Yin, Stability analysis for Li-ion battery model parameters and state of charge estimation by measurement uncertainty consideration, Energies 8 (8) (2015) 7729, http://dx.doi.org/10.3390/en8087729.
[24] A. Vahidi, A. Stefanopoulou, H. Peng, Recursive least squares with forgetting for online estimation of vehicle mass and road grade: theory and experiments, Veh. Syst. Dyn. 43 (1) (2005) 31–55, http://dx.doi.org/10.1080/00423110412331290446.
[25] Y. Hu, Y.Y. Wang, Two time-scaled battery model identification with application to battery state estimation, IEEE Trans. Control Syst. Technol. 23 (3) (2015) 1180–1188, http://dx.doi.org/10.1109/TCST.2014.2358846.

[26] S. Haykin, Kalman Filtering and Neural Networks, John Wiley & Sons, Inc., 2002, http://dx.doi.org/10.1002/0471221546.ch1.
[27] Z. He, M. Gao, C. Wang, L. Wang, Y. Liu, Adaptive state of charge estimation for Li-ion batteries based on an unscented Kalman filter with an enhanced battery model, Energies 6 (8) (2013) 4134, http://dx.doi.org/10.3390/en6084134.
[28] G.L. Plett, Recursive approximate weighted total least squares estimation of battery cell total capacity, J. Power Sources 196 (4) (2011) 2319–2331, http://dx.doi.org/10.1016/j.jpowsour.2010.09.048.
[29] L. Lam, P. Bauer, E. Kelder, A practical circuit-based model for Li-ion battery cells in electric vehicle applications, 2011 IEEE 33rd International Telecommunications Energy Conference (INTELEC) (2011) 1–9, http://dx.doi.org/10.1109/INTLEC.2011.6099803.